WATER RESOURCES RESEARCH, VOL. 43, W07409, doi:10.1029/2006WR005317, 2007

Topographic, meteorologic, and canopy controls on the scaling characteristics of the spatial distribution of snow depth fields

Ernesto Trujillo,[1] Jorge A. Ramírez,[1] and Kelly J. Elder[2]

Received 5 July 2006; revised 19 December 2006; accepted 30 April 2007; published 11 July 2007.

[1] In this study, LIDAR snow depths, bare ground elevations (topography), and elevations filtered to the top of vegetation (topography + vegetation) in five 1-km^2 areas are used to determine whether the spatial distribution of snow depth exhibits scale invariance, and the control that vegetation, topography, and winds exert on such behavior. The one-dimensional and mean two-dimensional power spectra of snow depth exhibit power law behavior in two frequency intervals separated by a scale break located between 7 m and 45 m. The spectral exponents for the low-frequency range vary between 0.1 and 1.2 for the one-dimensional spectra, and between 1.3 and 2.2 for the mean two-dimensional power spectra. The spectral exponents for the high-frequency range vary between 3.3 and 3.6 for the one-dimensional spectra, and between 4.0 and 4.5 for the mean two-dimensional spectra. Such spectral exponents indicate the existence of two distinct scaling regimes, with significantly larger variations occurring in the larger-scale regime. Similar bilinear power law spectra were obtained for the fields of vegetation height, with crossover wavelengths between 7 m and 14 m. Further analysis of the snow depth and vegetation fields, together with wind data, support the conclusion that the break in the scaling behavior of snow depth is controlled by the scaling characteristics of the spatial distribution of vegetation height when snow redistribution by wind is minimal and canopy interception is dominant, and by the interaction of winds with features such as surface concavities and vegetation when snow redistribution by wind is dominant.

Citation: Trujillo, E., J. A. Ramírez, and K. J. Elder (2007), Topographic, meteorologic, and canopy controls on the scaling characteristics of the spatial distribution of snow depth fields, *Water Resour. Res.*, *43*, W07409, doi:10.1029/2006WR005317.

1. Introduction

[2] Spatial heterogeneity has been identified as one of the main features of snow covers in several environments [e.g., *Elder et al.*, 1991; *Blöschl and Kirnbauer*, 1992; *Luce et al.*, 1998]. The spatial distribution of snow is controlled by precipitation patterns and the interaction of the snow with factors such as topography, slope, aspect, vegetation, shortwave and longwave radiation, and wind. These interactions result in a highly heterogeneous snow cover in space and in time. Accounting for this heterogeneity is of paramount importance for hydrologic modeling and for appropriately describing land surface–atmosphere interactions [e.g., *Luce et al.*, 1997, 1998; *Liston and Sturm*, 1998; *Liston*, 1999; *Liston et al.*, 1999; *Greene et al.*, 1999].

[3] Efforts to characterize this variability of snow properties have focused on exploring the statistical relationships between these properties and topographic variables that can be easily obtained by using digital elevation models (DEM's) and other computational tools. *Elder et al.* [1991] attempted to accurately determine the distribution of snow water equivalent (SWE) over a small alpine basin by identifying and mapping zones of similar snow properties on the basis of topographic and radiation parameters that account for variations in both accumulation and ablation. In their study, slope, elevation and radiation were used to obtain regressions of SWE as the dependent variable. Radiation consistently showed higher correlation with SWE, although weak correlations were obtained for all of the variables. *Blöschl and Kirnbauer* [1992] also studied the relationship between snow cover patterns and terrain characteristics, i.e., elevation and slope, in a mountainous area in the Austrian Alps. They noted an increase in snow covered area with increasing elevation and decreasing slope, although no unique relationship to terrain parameters was apparent. Similar examples of this type of study include *Evans et al.* [1989] and *Hosang and Dettwiler* [1991]. Although these approaches provide insight on how snow cover properties relate to each of these influencing variables, regression type relationships are only able to explain a small percentage of the variability, and no unique relationship can be defined for different environments because of differences in the dominant processes for different locations.

[4] The applicability of such relationships has been explored in the development of methodologies to spatially extrapolate variables, such as snow depth and snow water equivalent, throughout an area on the basis of information obtained from local and limited observations. Included in these efforts are the SWETREE model [*Elder et al.*, 1995, 1998; *Winstral et al.*, 2002], which uses binary decision

[1]Department of Civil and Environmental Engineering, Colorado State University, Fort Collins, Colorado, USA.
[2]Rocky Mountain Research Station, U.S. Department of Agriculture Forest Service, Fort Collins, Colorado, USA.

0043-1397/07/2006WR005317$09.00

trees to estimate SWE and snow depth on the basis of redistribution indices, terrain features and radiation. Other approaches involve the application of subgrid parameterizations of snow distribution, using depletion curves to relate snow covered area with normalized snow water equivalence [*Luce et al.*, 1999; *Luce and Tarboton*, 2001, 2004], and the complex mean geostatistical methodology [*Erickson et al.*, 2005], which uses a kriging scheme with a nonlinear trend model to interpolate snow depth measurements. *Erxleben et al.* [2002] compared several of these spatial interpolation methods for estimating snow distribution in the Colorado Rocky Mountains. Snow depths measured on three 1-km^2 areas were interpolated by using inverse distance weighting, ordinary kriging, modified residual kriging and cokriging, and binary regression trees. Additionally, snow density samples were interpolated by using linear regressions with elevation, slope, aspect, and net solar radiation, and SWE estimates were obtained by combining these two variables. They found binary regression trees to provide the most accurate estimates of snow depth; however, substantial portions of the variability were left unexplained by the models and none of them outperformed the others in all of the environments. These results illustrate the necessity for a better and more accurate characterization of the spatial and temporal organization of snow cover properties, focusing on the characteristics of the variability for different environments. *Blöschl* [1999] addresses several issues related to the accurate representation of snow cover properties, and the relationships between processes, measurement and model scales. Answers to questions about the nature of the spatial variability of snow properties across several scales, and about how this variability determines the scales at which snow measurements should be obtained still need to be addressed in order to improve our understanding of snow processes and to accurately represent snow cover properties in hydrologic applications.

[5] In recent years, the concepts of fractals and scale invariance have been introduced to analyze the spatial and temporal structure of variables such as rainfall [e.g., *Lovejoy and Schertzer*, 1985; *Tessier et al.*, 1993; *Over*, 1995; *Over and Gupta*, 1996; *Marsan et al.*, 1996; *Kang and Ramírez*, 2001], soil moisture [e.g., *Rodríguez-Iturbe et al.*, 1995], topography [e.g., *Mandelbrot*, 1967, 1982; *Brown*, 1987; *Turcotte*, 1987, 1989; *Huang and Turcotte*, 1989], drainage network slopes [e.g., *Tarboton et al.*, 1988; *Rodríguez-Iturbe and Rinaldo*, 1996; *Molnar and Ramírez*, 1998], and steady state and transient infiltration rates [e.g., *Meng et al.*, 1996]. In the case of snow properties, these concepts have been applied in the analysis of snow-covered area [e.g., *Shook et al.*, 1993; *Shook and Gray*, 1997; *Blöschl*, 1999; *Granger et al.*, 2002], snow depth [e.g., *Shook and Gray*, 1994, 1996 and 1997; *Kuchment and Gelfan*, 2001; *Deems et al.*, 2006] and SWE [e.g., *Shook and Gray*, 1997], indicating that such variables exhibit fractal characteristics within a finite range of spatial scales.

[6] *Shook et al.* [1993] analyzed the perimeter-area and area-frequency relationships of snow and soil patches of melting snow covers in prairie and alpine environments for different stages during the melting season suggesting that snow and soil patches are fractals. They conclude that snow patches are not random and their size distribution is predictable and can be described by the use of simple power law equations characterized by their fractal dimension. *Granger et al.* [2002] made use of these power law relationships to describe snow and soil patches characteristics in the development of a methodology to determine the amount of energy removed by the snow patch surface as warmer air moves over it. *Shook and Gray* [1994, 1996] analyzed the fractal nature of snow depth in shallow snow covers by looking at the variation in the standard deviation of snow depth transects as a function of sample distance. Their results indicate a power law type increase in the standard deviation up to sampling distances of the order of 20 m, after which the relationship curves toward a horizontal slope in the log-log plot. They conclude that this segmented power law shape relationship indicates that the spatial distribution of snow depth is fractal at small scales (<30 m) and random at scales larger than this threshold, and that the cutoff length is related to the macroscopic (>100 m) variability of topography. On the basis of these findings, *Shook and Gray* [1997] implemented a methodology for generating a synthetic snow cover that forms snow patches having fractal properties, on the basis of a fractal sum of pulses technique. In their methodology, the synthetic data generated with the fractal technique are adjusted to resemble the characteristics of natural snow covers by adjusting the generated frequency distribution to that estimated from field measurements. The statistical properties of the generated snow covers agree well with those of the measured fields, supporting the application of fractal techniques for synthetic generation of snow cover properties. *Kuchment and Gelfan* [2001] extended the analysis of snow depth to straight-line courses from 100 m to several kilometers in length to represent the microscale and mesoscale variability in several types of landscapes and relief, obtaining power law relationships in the variograms concluding that the snow depth fields could be considered statistically self-similar. Similar results were obtained by *Arnold and Rees* [2003] from the analysis of semivariograms of snow depth courses in glacier surfaces, concluding that snow depth distributions on glacier environments also exhibit fractal properties at short spatial separations and become random as separation increases.

[7] In a recent publication, using data derived from Light Detection and Ranging (LIDAR) observations, *Deems et al.* [2006] analyze the variograms of snow depth, topography and vegetation topography of three 1-km^2 study areas with a strong influence of snow redistribution by wind. From the observed log-log linearity of the variograms, they infer fractal behavior in the elevation, vegetation topography (elevation + vegetation height) and snow depth data sets. Their analyses seem to indicate the existence of two distinct scale regions with fractal distributions for the snow depth and vegetation topography data sets, separated by a scale break that varies between 15 m and 40 m for snow depth, and between 31 m and 56 m for vegetation topography, similar to the results obtained by *Shook and Gray* [1994, 1996], *Kuchment and Gelfan* [2001], and *Arnold and Rees* [2003]. The fractal dimensions obtained for snow depth are of the order of 2.5 for the shorter scale range and 2.9 for the longer scale range. From these values, *Deems et al.* [2006] infer that for the short range there is a balance between high- and low-frequency variations, while at larger distances the

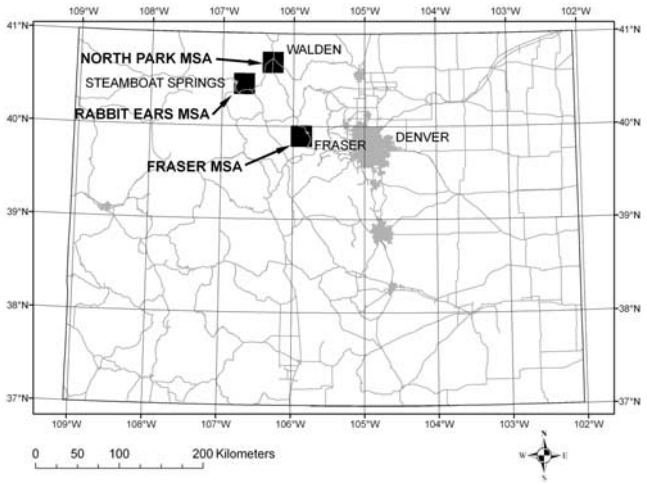

Figure 1. Location of the mesoscale study areas of the Cold Land Processes Experiment (CLPX) within the state of Colorado (United States).

distribution of snow depth approaches a spatially random distribution. Regarding the location of the breaks, *Deems et al.* [2006] speculate that the length of the scale break might be related to the overall terrain relief, and that the process change revealed by the breaks in the variograms of the vegetation topography (topography + vegetation height) data potentially influences the scaling behavior of snow depth. From relatively small variations of the fractal dimensions for different directions of the order of 0.1 in the snow depth, *Deems et al.* [2006] conclude that such variations show a strong qualitative relationship to prevailing winds and large-scale topographic orientation.

[8] In this study, the spatial scaling characteristics of snow depth are explored on the basis of the analysis of the power spectral densities of high-resolution LIDAR measurements ($\sim$1 m) distributed within five 1-km^2 areas (two of them used by *Deems et al.* [2006]) with significant differences in the characteristics of the spatial variability of the snow cover caused by differences in terrain, vegetation, and wind patterns. Spectral analyses are performed on the 1-km^2 raster fields of snow depth, topography, topography + vegetation height, and vegetation height. The data set used in this study not only includes environments in which redistribution of snow by wind is dominant, but also includes environments in which snow redistribution is minimal and canopy interception of snowfall is dominant, allowing for the identification of differences in the spectral characteristics between these two types of environments. The results from the power spectral analysis are complemented by an analysis of maximum wind speeds and directions, and of the separation distance between peaks in the snow depth and vegetation height profiles. Also, the spectral characteristics (e.g., spectral exponents) are compared to wind patterns in search for any relationship between the two. Throughout section 5, the results and conclusions obtained in this study are compared to those obtained in the previous point data studies, and in particular those presented by *Deems et al.* [2006], pointing out the new insights in the actual knowledge of the spatial variability of snow depth provided by the results presented here not pointed out in the published literature. A summary description of the scale invariance concepts applied in this study is included in Appendix A.

2. Field Description and Data Set

[9] The data used in this study were collected as part of the Cold Land Processes Experiment (CLPX) in 2003. The CLPX was a cooperative effort of NASA, NOAA and other government agencies and universities designed to advance the understanding of the terrestrial cryosphere, providing information to address questions on cold land processes, spatial and temporal variability of the snow cover, and uncertainty of remote sensing measurements and models (D. Cline and Cold Land Processes Working Group, Cold Land Processes field experiment plan, 2001, available at http://www.nohrsc.nws.gov/~cline/clpx.html). The study area of the CLPX is conformed by a nested array of study areas at five different scale levels in the state of Colorado and a small portion of southern Wyoming (Figure 1). The two first levels correspond to one large and one small regional study areas of 3.5° × 4.5° and 1.5° × 2.5°, respectively. Three Meso-cell study areas (MSA) of 25 km × 25 km and nine 1 km × 1 km intensive study areas (ISA's) conform the third and fourth scale levels, respectively. The last scale level corresponds to one local-scale observation site (LSOS) of 1 ha. This study focuses on five of the nine 1-km^2 ISA's. The ISA's located in the North Park MSA were not included in this study because their snow-covered area is less than 35% in all cases, while the Alpine ISA located in the Fraser MSA is analyzed in a separate study to illustrate differences between snowpack characteristics in alpine and subalpine environments. The areas included here correspond to the Fool Creek (FF) and Saint Louis Creek (FS) ISA's located in the Fraser MSA, and the Buffalo Pass (RB), Spring Creek (RS), and Walton Creek (RW) ISA's located in the Rabbit Ears MSA. A summary of the major characteristics of these areas is presented in Table 1.

[10] The Fool Creek ISA is located in a forested area with a complex topography and variations in vegetation characteristics. Elevations range between 3014 m above sea level (asl) and 3284 m asl. The ISA is part of the area of the Fraser Experimental Forest where extensive research has been performed on the effect of forest management practices on runoff. These forest management practices have led to a pattern of plots of cut and leave strips that produced differences in coniferous vegetation height. The Saint Louis Creek ISA is located at the lower part of the Fraser Experimental Forest. Elevations range between 2701 m asl and 2756 m asl. The area presents mild slopes and a uniform coniferous forest cover, except for some small patches of open terrain. The Buffalo Pass ISA has an elevation range of 3053 m asl to 3233 m asl. A stream that flows from east to west divides the area into a north facing and a south facing slopes. The Spring Creek ISA is an area with a more complex topography. The minimum and maximum elevations are 2668 m asl and 2903 m asl. Aspect variations are a major feature in this ISA, with several south and north facing slopes spread over the area. Vegetation cover consists of dense patches of deciduous vegetation, and only a few clusters of coniferous trees. The rest of the area is covered by short vegetation and grass. Finally, the Walton Creek ISA is characterized by mild slopes and open areas. Elevation ranges between 2915 m asl and 2998 m asl. A small percentage of the ISA is covered by

Table 1. Major Characteristics of the Intensive Study Areas (ISA's)[a]

Name	Site	Characteristics
Fool Creek	FF	moderately high-density coniferous (spruce-fir) forest, on wet north facing slope
St. Louis Creek	FS	moderate density coniferous (lodgepole pine) forest, on a flat aspect with low relief
Buffalo Pass	RB	dense coniferous forest interspersed with open meadows; low rolling topography with deep snow packs
Spring Creek	RS	moderate density deciduous forest (aspen); moderate topography on west facing slope, with moderate snow packs
Walton Creek	RW	broad meadow interspersed with small, dense stands of coniferous forest; low rolling topography with deep snow packs

[a]Source is D. Cline and Cold Land Processes Working Group (Cold Land Processes field experiment plan, 2001, available at http://www.nohrsc.nws.gov/~cline/clpx.html).

coniferous vegetation, and the valleys are mostly covered by sage and willow shrubs.

[11] This study makes use of LIDAR topographic maps collected for each of the ISA's for snow-covered and snow-free conditions. The data set consists of LIDAR elevation returns (filtered to bare ground/snow, and filtered to top of vegetation), elevation contours (0.5 m), and snow depth contours (0.1 m) [*Miller*, 2003]. These data were processed from the LIDAR elevation returns with an average horizontal spacing of 1.5 m and vertical tolerance of 0.05 m. The snow depth contours were obtained by subtracting the two topographic surfaces corresponding to snow-covered conditions close to maximum accumulation (8–9 April 2003) and no-snow conditions (18–19 September 2003). The contour covers were used to generate Triangulated Irregular Network (TIN) surfaces of the fields in ArcGIS, which then were converted to rasters of 1024 by 1024 grid cells covering the entire 1-km^2 areas with a grid spacing of approximately 1 m for snow depth, bare ground elevations (topography), and elevation to the top of vegetation (topography + vegetation).

3. Methods of Analysis

3.1. One-Dimensional Power Spectra

[12] One-dimensional power spectra were obtained separately for each of the west to east (x) rows and each of the north to south (y) columns of the fields on each of the ISA's by following the procedure described below. First, the complex coefficients of the discrete Fourier transform of the original series or signal were determined by using:

$$X(k) = \frac{1}{N}\sum_{n=0}^{N-1} x(n)\exp[-j(2\pi/N)nk] \quad (1)$$

where k is the wave number (from 0 to $N/2$), N is the total number of data points in the discrete signal $x(n)$, and j is the square root of -1. The power spectrum was then estimated by obtaining the square of the absolute value of the complex coefficients of the discrete Fourier transform as

$$\phi(k) = |X(k)|^2 \quad (2)$$

where ϕ (k) is the power spectrum of the function $x(n)$. If the mean of the original signal is subtracted from the signal, the sum of the power spectrum over the entire range of frequencies equals the variance of the process. In this way, the power spectrum represents the absolute contribution of each frequency (or scale) to the total variance of the process. If the power spectrum is then divided by the variance, a power spectral density is obtained, where the value of the spectrum corresponds to the percentage of the total variance contributed by each frequency. The individual power spectral densities of the profiles in the x and y directions were then averaged over each direction, reducing the variability of the individual spectra and facilitating the fitting of power laws.

3.2. Directional One-Dimensional Power Spectra

[13] In order to examine anisotropic behavior, that is, changes of the behavior of the power spectra of snow depth as a function of direction, this analysis makes use of directional rasters for which the directions of the x and y coordinates of the lattice coincide with the directions for which the analysis is performed. For example, a rotation of the snow depth contours of 30° with respect to the west to east axis allows for the analysis of the power spectra for a 30°–210° (x axis) direction, and for a 120°–300° (y axis) direction. These lines correspond to two perpendicular directions, similar to rotating the east-west and north-south axes by an angle of 30°. These rasters were generated for even intervals of 10° (i.e., 0°–180°, 10°–190°, 20°–200°, ..., 170°–350° with respect to the east axis; equivalent to E–W, N 80°E–S 80°W, N 70°E–S 70°W, ..., N 80°W–S 80°E). Because the power spectral analysis must be performed on a square grid, the rotations of the contour maps cause a reduction of the available information to a grid of 512 × 512 cells (next power down from 2^{10}) centered in the area. The one-dimensional power spectra for each direction were obtained by following the procedure described in section 3.1.

3.3. Mean Two-Dimensional Power Spectra

[14] A similar procedure is followed for the two-dimensional spectral analysis. First, the two-dimensional discrete Fourier Transform is estimated by using

$$X(k,l) = \frac{1}{N^2}\sum_{m=0}^{N-1}\sum_{n=0}^{N-1} x(m,n)\exp\left[-j\frac{2\pi}{N}(km+ln)\right] \quad (3)$$

where k and l are the wave numbers in the x and y directions (from 0 to $N/2$), N is the total number of data points in both

the x and y directions, and $x(m, n)$ is the original function. The two-dimensional power spectrum is then obtained by

$$\phi(k,l) = |X(k,l)|^2 \tag{4}$$

[15] The power spectral densities of the fields were obtained by dividing the power spectra by the variance. These two-dimensional power spectral densities were used to obtain mean two-dimensional power spectral densities. An equivalent wave number is assigned to each ϕ (k, l) following

$$r = \frac{1}{L}\left(k^2 + l^2\right)^{1/2} \tag{5}$$

where L is the dimension of the side of the square area for which the analysis is being performed (1000 m in this case). The mean spectral density ϕ_j for each equivalent wave number r is given by

$$\phi_j = \frac{1}{N_j}\sum_{i=1}^{N_j} |X_i(k,l)|^2 \tag{6}$$

where N_j is the number of values that satisfy the condition $j/L < r < (j + 1)/L$, and the summation is carried out over all the coefficients located in this frequency range.

4. Results

4.1. Snow Depth

4.1.1. One-Dimensional Power Spectra

[16] The log-log plots of the one-dimensional power spectral densities of snow depth are presented in Figure 2. None of the one-dimensional power spectra present log-log linearity throughout the entire range of frequencies, although they can be subdivided into two frequency intervals within which the spectra is well represented by a power law. The scale break in each of the sites splits the power spectrum in a low-frequency (larger-scale) interval with a mild slope, and a high-frequency (smaller-scale) interval with a steeper slope. These power spectra with segmented power law indicate that the characteristics of the spatial variability of snow depth can be classified in different frequency regions or scale intervals within which the self-affinity condition (A3) (see Appendix) is met. A summary of the average spectral exponents and scale breaks is presented in Table 2. The wavelengths that separate these two intervals vary between 8 m and 35 m, with the smallest breaks at Fool Creek, Saint Louis Creek and Spring Creek. For these sites, little difference is observed in the crossover wavelengths in the x and y directions. On the contrary, the corresponding x and y crossover wavelengths for the Buffalo Pass and Walton Creek fields differ 12 m and 13 m, respectively, indicating some degree of anisotropy on the variability of these snow depth fields. The spectral exponents obtained vary between 0.2 and 1.4 for the low-frequency intervals, and between 3.1 and 3.6 for the high-frequency intervals. These large differences between the spectral exponents of the larger and smaller-scale intervals indicate marked differences in the nature of the variability of the snow depth cover above and below the scale break. Such differences are addressed in the discussion section.

4.1.2. Directional One-Dimensional Power Spectra

[17] The distributions of the spectral exponents and scale breaks of snow depth are summarized in Figure 3 and Table 3. The spectral exponents (Figure 3a) vary between 0.06 and 1.17 for the low frequencies, and between 2.93 and 3.58 for the high frequencies. Little variations are observed in the high-frequency values with respect to those observed in the corresponding low-frequency exponents. Average values range between 0.4 and 1.1 for the low frequencies, and between 3.1 and 3.4 for the high frequencies. The smallest and largest average exponents are found at Buffalo Pass and Spring Creek for the low frequencies, and at Walton Creek and Saint Louis Creek for the high frequencies, respectively. The crossover wavelengths (Figure 3b) are located at scales of the order of meters and tens of meters. The scale breaks at Fool Creek, Saint Louis Creek and Spring Creek present little variation around the mean, with average breaks between 9 m and 12 m. In contrast, the breaks at Buffalo Pass and Walton Creek exhibit larger variations and are located at larger scales that range between 19 m and 45 m, with average values of 21 m and 34 m, respectively. These variations indicate a more significant heterogeneity and directionality in the snow covers of these two areas.

4.1.3. Mean Two-Dimensional Power Spectra

[18] The mean two-dimensional power spectral densities of snow depth are presented in Figure 4. Spectral exponents and scale breaks are summarized in Table 4. Consistent with the results of the one-dimensional spectra, the break in the scaling of snow depth is observed at wavelengths between 7 m and 22 m. At Fool Creek, Saint Louis Creek and Spring Creek, the breaks occur at wavelengths between 7 m and 9 m, while at Buffalo Pass and Walton Creek they occur at 18 m and 22 m, respectively. The spectral exponents vary between 1.3 and 2.2 for the low frequencies, and between 4.0 and 4.5 for the high frequencies. These spectral exponents for both intervals differ approximately by a unit with respect to the corresponding one-dimensional exponents.

4.2. Topography and Topography Plus Vegetation Height

4.2.1. One-Dimensional Power Spectra

[19] The power spectra of topography in all of the study areas behave like $k^{-\beta}$ for the entire range of frequencies. The spectral exponents vary between 1.99 and 2.02, with almost no variations from site to site. Similar scaling behavior has been observed in previous studies of topographic profiles and contour lines, illustrating the vertical self-affinity and horizontal self-similarity of topography [e.g., *Mandelbrot*, 1967, 1982; *Brown*, 1987; *Turcotte*, 1987, 1989; *Huang and Turcotte*, 1989]. In these studies, spectral exponents around 2.0 were found for one-dimensional topographic profiles. Complementarily, the spectra of topography + vegetation height exhibit a distortion of the power law relationship with frequency observed in the spectra of topography. This distortion is more evident at Fool Creek and Saint Louis Creek, which are characterized by taller and denser vegetation. Also, the distortion is sometimes more evident in one of the two directions because of differences in the relative contribution of vegetation to the variability/roughness of

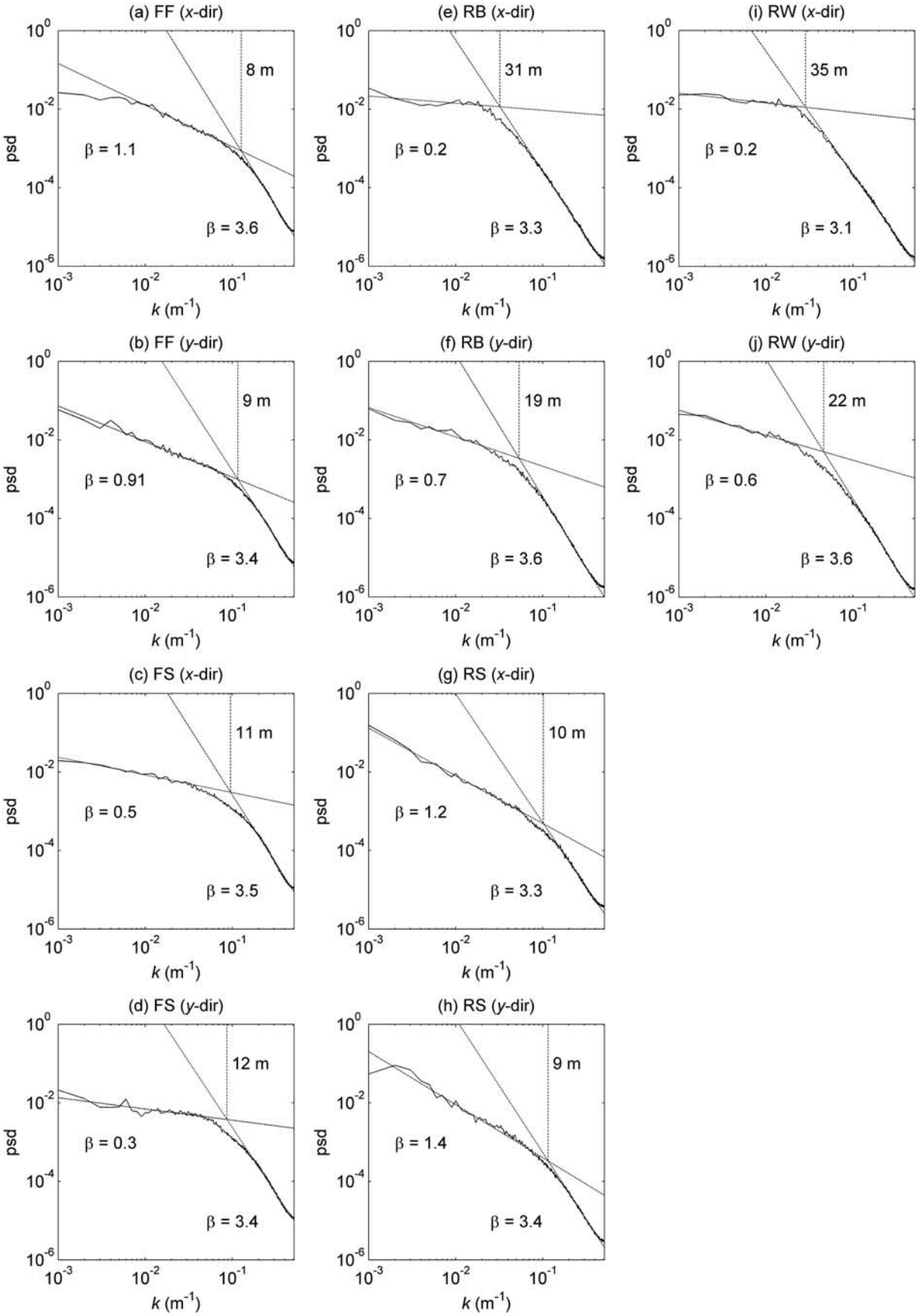

Figure 2. Average one-dimensional power spectral densities of snow depth in the east-west (x dir) and north-south (y dir) directions; k is the wave number divided by the length of the profiles (1000 m).

Table 2. Average Spectral Exponents and Scale Breaks of Snow Depth From the One-Dimensional Analysis of the Nonrotated Rasters[a]

	FF	FS	RB	RS	RW
Low-frequency β	1.0	0.4	0.5	1.3	0.4
High-frequency β	3.5	3.4	3.5	3.3	3.3
Scale break, m	8	11	25	9	28

[a]1024 × 1024.

the profiles along each direction. When vegetation height is of a similar order of magnitude as the elevation range, the contribution of vegetation to the total variance of the profile increases, leading to a more noticeable distortion in the power spectrum at the smaller scales. On the contrary, when the elevation range is greater than vegetation height, the contribution of vegetation to the variability of the profile is reduced, and little distortion in the power spectrum is perceived. These differences are more evident at Fool Creek, Saint Louis Creek, and Walton Creek, where the elevation range is greater in one direction than in the other.

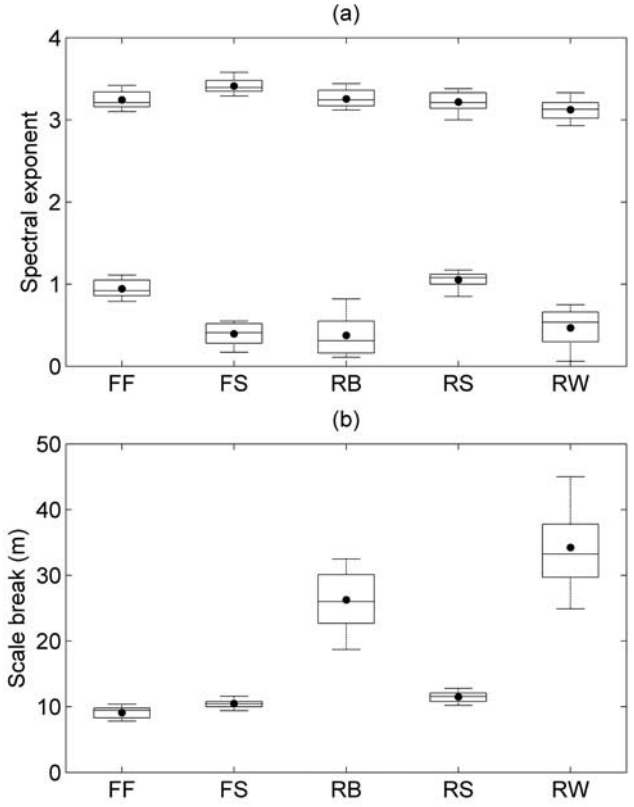

Figure 3. Distribution of the characteristics of the directional power spectral densities of snow depth in all possible directions. (a) Spectral exponents for the lower frequencies (smaller values) and higher frequencies (larger values) intervals and (b) scale breaks. The external lines cover the entire range of the data, the lower and upper limits of the box mark the 0.25 and 0.75 percentiles, while the internal line marks the median. The dots correspond to the mean of the set.

None of the scale breaks in the power spectra of snow depth can be observed in the power spectra of bare ground elevations, or in the spectra of topography + vegetation. Neither the power spectrum exponents nor the scale breaks of the snow depth fields can be explained on the basis of the power spectrum of the underlying topography and topography + vegetation. If the scale break in the scaling characteristics of snow depth observed at the smaller scales is the product of a switch in the dominant process(es) driving the variability of the snow cover properties, this change is not, at least evidently, explained by the spectral characteristics of either the underlying topography or topography + vegetation.

4.2.2. Directional One-Dimensional Power Spectra

[20] The power law exponents of the directional spectra of topography vary between 1.94 and 2.1, with an average of 2.0. Little anisotropy is perceived in the characteristics of the directional spectra. The inclusion of vegetation height in the topographic profiles induces a distortion of the power law relationship in all directions. No scale breaks are observed in the directional spectra of topography or topography + vegetation.

4.2.3. Mean Two-Dimensional Power Spectra

[21] Spectral exponents between 2.92 and 2.94 were obtained for the mean two-dimensional power spectra of topography, which differ approximately by a unit with respect to the one-dimensional values. Such spectral exponents are consistent with similar analyses of the mean two-dimensional power spectra of topography [e.g., *Huang and Turcotte*, 1989], in which an average exponent of 2.82 was found for different types of topography.

4.3. Vegetation

4.3.1. One-Dimensional Power Spectra

[22] The average one–dimensional power spectra of vegetation height are presented in Figure 5 and the spectral exponents and scale breaks are summarized in Table 5. Vegetation exhibits similar scaling characteristics as the corresponding snow depth covers. A low-frequency interval with mild slopes and a high-frequency interval with steeper slopes are separated by a scale break located at wavelengths between 7 m and 16 m. The spectral exponents vary between 0.3 and 1.2 for the low frequencies, and between 1.9 and 3.4 for the high frequencies. The breaks at the Fool Creek, Saint Louis Creek and Spring Creek differ from those in the snow depth scaling between 0 m and 3 m, while at Buffalo Pass and Walton Creek the differences vary between 9 m and 15 m, with breaks at larger scales for snow depth. There is a difference in the scaling behavior of

Table 3. Average Spectral Exponents and Scale Breaks of Snow Depth From the Directional One-Dimensional Analysis[a]

	FF	FS	RB	RS	RW
Low-frequency β					
Mean	0.9	0.4	0.4	1.1	0.5
Standard deviation	0.11	0.12	0.23	0.09	0.23
High-frequency β					
Mean	3.2	3.4	3.3	3.2	3.1
Standard deviation	0.10	0.09	0.11	0.12	0.11
Scale break, m					
Mean	9	10	26	12	34
Standard deviation	0.9	0.6	4.1	0.8	6.2

[a]512 × 512.

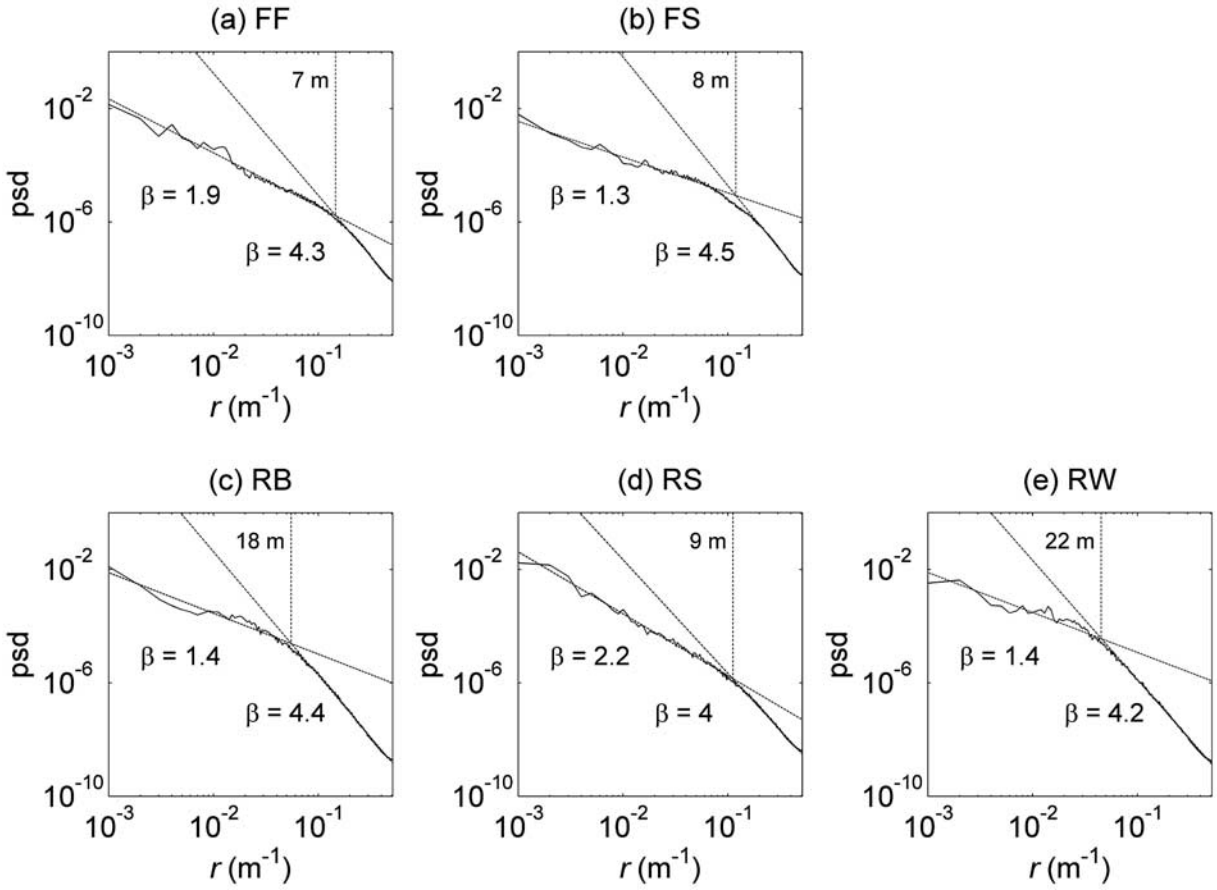

Figure 4. Mean two-dimensional power spectral densities of snow depth for all of the study areas; r is the equivalent wave number as in (5).

the snow covers of these last two areas with respect to that of the corresponding vegetation covers.

4.3.2. Mean Two-Dimensional Power Spectra

[23] The spectral exponents and scale breaks in the mean two-dimensional spectra of vegetation height are summarized in Table 6. The scale breaks are located between 7 m and 11 m, and the slopes vary between 1.1 and 2.0 for the low frequencies and between 2.9 and 4.3 for the high frequencies. The breaks at Buffalo Pass and Walton Creek differ from those in the mean two-dimensional spectra of snow depth by 7 m and 13 m, respectively. The spectral exponents of snow depths for each of the intervals do not correspond exactly to the exponents of vegetation heights because of the differences between the magnitudes of the variations of the snow depth cover and those of the corresponding vegetation cover at each scale.

5. Discussion

[24] Overall, the results from the spectral analyses of snow depth indicate the existence of two distinct scaling regimes within the interval between 1 m and 1 km, each characterized by a distinct spectral exponent. These two regimes are separated by a scale break located at scales of the order of meters to tens of meters. The existence of these scaling regimes is caused by differences in the characteristics of the variability above and below the break. Within each interval, the power spectrum follows a power law dependence on frequency indicating self-affinity in the snow depth covers within finite frequency/scale intervals. This type of scaling behavior with segmented power law spectrum, referred to as bilinear (two intervals) or multilinear (multiple intervals) [*Veneziano and Iacobellis*, 1999], has been observed in several other processes such as rain rate [*Crane*, 1990] and groundwater base flow [*Zhang and Schilling*, 2004; *Zhang and Li*, 2005]. For the case of rain rate, *Crane* [1990] associates the changes in the spectral exponents and the wave numbers at which these breaks occur with the characteristics of the two-dimensional turbulent processes that determine the spatial distribution of rainfall. *Zhang and Schilling* [2004] and *Zhang and Li* [2005] obtained similar bilinear power spectra for estimated time series of base flow on five different rivers in the state of Iowa (United States). They conclude that the high-frequency variations of the base flow are related to individual rainfall events ranging from a few hours to a few days,

Table 4. Exponents and Scale Breaks for the Mean Two-Dimensional Power Spectra of Snow Depth

	FF	FS	RB	RS	RW
Low-frequency β	1.9	1.3	1.4	2.2	1.4
High-frequency β	4.3	4.5	4.4	4.0	4.2
Scale break, m	7	8	18	9	22

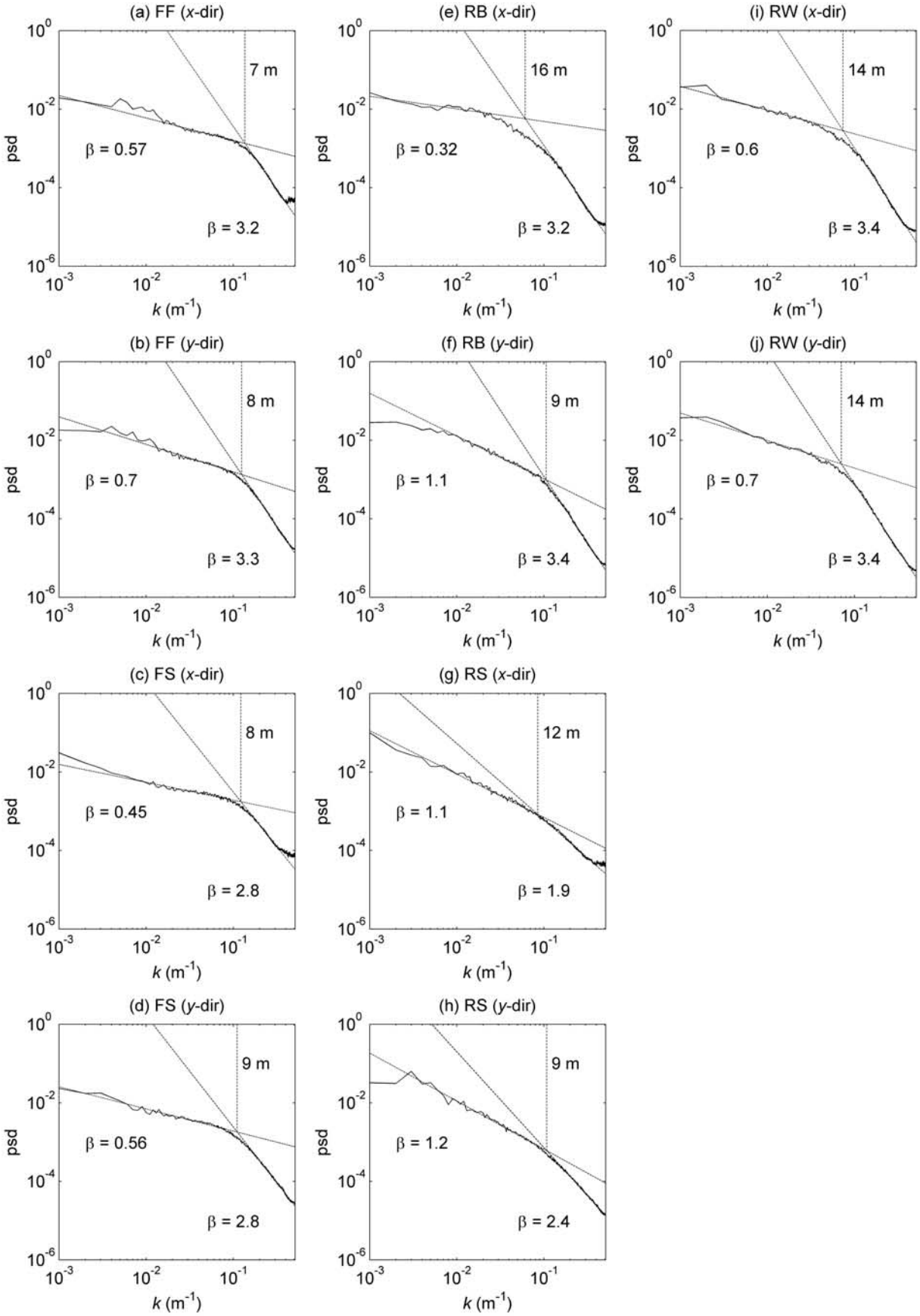

Figure 5. Average one-dimensional power spectral densities of vegetation in the east-west (x dir) and north-south (y dir) directions; k is the wave number divided by the length of the profiles (1000 m).

Table 5. Spectral Exponents and Scale Breaks of Vegetation From the One-Dimensional Spectral Analysis

	FF	FS	RB	RS	RW
Low-frequency β	0.6	0.5	0.7	1.2	0.7
High-frequency β	3.2	2.8	3.3	2.2	3.4
Scale break, m	8	9	13	11	14

while the low-frequency variations are the result of seasonal changes.

[25] For the case of snow depth, similar scale breaks have been observed in previous studies of point data. *Shook and Gray* [1994, 1996] analyzed the standard deviation of snow depth transects in prairie and artic environments as a function of sample size ($\sim$ sample distance), covering distances up to 1200 m. Their results indicate a power law type increase in the standard deviation up to sampling distances of the order of 20 m, after which the relationship curves toward a slope of 0.06 in the log-log plot. *Shook and Gray* [1996] defined a cutoff length as the point of intersection between the initial slope and a horizontal tangent to the end of the curve in the log-log plot of standard deviation versus sample distance. This definition is used to compare the scale at which the break occurs in different environments, extending the analysis to transects in two other areas with variations in elevation range. Cutoff lengths between 30 m and 500 m were obtained for the three environments. *Arnold and Rees* [2003] obtained similar results from the analysis of semivariograms of snow depth courses in glacier surfaces. Their results indicate an increase in the variance with separation under scales between 20 m and 30 m in the summer, and between 35 m and 45 m in the spring, after which the semivariograms reach a reasonably flat sill. In a more recent study, *Deems et al.* [2006] analyzed the variograms of the LIDAR snow depths of the Buffalo Pass, Walton Creek and Alpine ISA's. Their results indicate a similar bilinear behavior with a break at scales between 15 m and 40 m. However, *Deems et al.* do not present any conclusive evidence of the link between such bilinear behavior and the physical processes driving the variability of snow depth. Later in this discussion, the relationship between the observed bilinear behavior of the power spectrum of snow depth and controlling variables such as vegetation and wind patterns is determined on the basis of additional analysis of the vegetation height fields and wind data in each of the study areas.

[26] The one-dimensional spectral exponents obtained for snow depth vary between 0.1 and 1.4 for the low-frequency intervals, and between 2.9 and 3.6 for the high-frequency intervals. Such low-frequency exponents indicate that for points separated by distances larger than the corresponding scale break, the snow depth values are weakly correlated, although the correlation is not necessarily zero, and there is some weak long-range persistence. In contrast, the high-frequency exponents indicate that snow depth values for points separated by distances smaller than the corresponding scale break are highly correlated, and that the snow depth surface becomes smoother below the scale break. The variability is significantly different above and below the break. This spatial organization of snow depth within these two scale intervals is described differently in previous studies. *Shook and Gray* [1994, 1996] describe the distribution of snow depth as fractal below scales between 20 m and 100 m, and random above such scales, on the basis of slope values in the log-log plots of snow depth versus sampling distance of 0.47 for the short-range interval, and 0.06 for the long-range interval. Similarly, *Arnold and Rees* [2003] conclude from the flattening of the log-log semivariograms of snow depth above separation distances between 10 m and 45 m that snow depth distributions show fractal properties at short separations, and become random as separation increases. *Deems et al.* [2006] also suggest, from fractal dimensions of around 2.5 for the short range and 2.95 for the long range, that the snow depth distributions exhibit fractal properties at short spatial separations and become almost random above the corresponding scale breaks. The scale breaks found in this study are located within the same orders of magnitude as those found in the quoted studies, although the spectral exponents for the low frequencies indicate that the distribution of snow depth at scales larger than the corresponding break is not completely random, if the term "random" is used to refer to processes of the white noise type which exhibit horizontal power spectra ($\beta = 0$), indicating equal contributions from all frequencies to the total variance. The results obtained in this study indicate the existence of some organization at scales larger than the scale break such that the contribution of each frequency to the total variance can be described by a power law, with an average spectral exponent (including all sites) of 0.65 for the one-dimensional case, and 1.64 for the two-dimensional case. Such exponents indicate a decaying contribution of each frequency to the total variance. This organization is site dependent, and although some of the sites present spectral exponents that are closer to zero, the range of exponents found indicates that the distribution of snow depths above a characteristic scale of the order of meters to tens of meters cannot be generalized as random or uncorrelated.

[27] As expected (see Appendix A), the exponents of the mean two-dimensional spectra for the two frequency regions (i.e., the low and high frequencies) differ approximately by one with respect to the one-dimensional exponents. Such difference is consistent with the theoretical difference between the exponents of the one-dimensional and two-dimensional power spectra for self-affine fields where all directions in the x-y plane are equivalent, i.e., no scaling anisotropy in the x-y plane (e.g., Appendix A) [*Voss*, 1985b]. When compared to the directional one-dimensional exponents, the exponents of the mean two-dimensional spectra for the low frequencies differ between 0.6 and 1.3 for Buffalo Pass, and between 0.7 and 1.4 for Walton Creek. On the other hand, such differences vary between 0.8 and 1.1 at Fool Creek, between 0.7 and 1.1 for Saint Louis Creek, and between 1.0 and 1.3 for Spring Creek. The range

Table 6. Exponents and Scale Breaks for the Mean Two-Dimensional Power Spectra of Vegetation Height

	FF	FS	RB	RS	RW
Low-frequency β	1.1	1.4	1.3	2.0	1.7
High-frequency β	3.8	3.3	4.2	2.9	4.3
Scale break, m	7	7	11	9	9

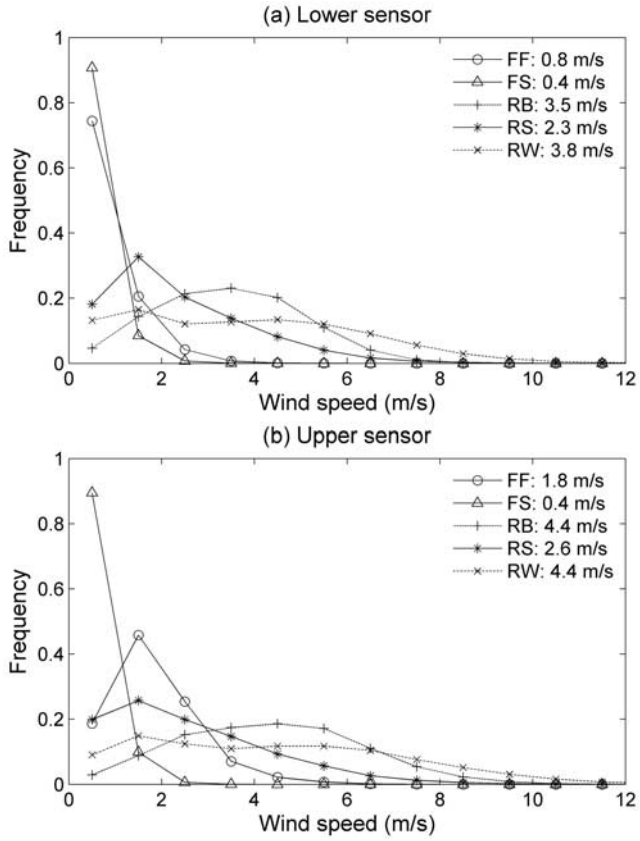

Figure 6. Empirical distribution functions of maximum wind speed every 10-min intervals for the period October 2002 to April 2003 measured within each intensive study area (ISA) at (a) 1 m above the maximum expected snow depth (lower sensor) and (b) 10 m above the ground (upper sensor). Only data for intervals with air temperature lower than 0°C are included. Average values are included in the legends.

of variation of the difference between the exponents of the mean two-dimensional spectra and one-dimensional spectra for the low frequencies is larger for the Buffalo Pass and Walton Creek areas, indicating a more significant scaling anisotropy in such fields for the larger scales. On the contrary, no significant scaling anisotropy is observed in the high-frequency exponents for all of the areas, with ranges of variation of the order of 0.3 in all of the five ISA's.

[28] In search for explanations for the observed segmented power law spectrum of snow depth, a similar scaling analysis was performed on the fields of topography, topography + vegetation and vegetation height. The topographic fields contain information about the variations in elevation, slope, and surface roughness which affect precipitation patterns, wind dynamics, redistribution of snow by avalanches, and energy fluxes due to variations in slope and aspect, among others. The fields of vegetation height contain information about the small-scale characteristics of the vegetation cover such as the separation between individual trees, height and area covered by the foliage, as well as larger-scale characteristics such as the location of tree clusters and their average characteristics. Such properties have a strong influence in the distribution of snow through processes such as canopy interception of snowfall and the interaction with wind. The topography + vegetation fields provide information about the combination of such controls. None of the breaks in the slope of the log-log spectra of snow depth are present in the power spectra of the corresponding fields of topography and topography + vegetation. Neither the power spectrum exponents nor the scale breaks can be explained on the basis of the power spectrum of the underlying topography and topography + vegetation. On the other hand, vegetation height exhibits very similar scaling behavior as the snow depth fields with bilinear power spectrum and scale breaks at wavelengths between 7 m and 14 m, with mild slopes for the low frequencies, and steeper slopes for the high frequencies (Figure 5).

[29] The study areas can be separated into two groups according to the similarities or differences between the locations of the scale breaks in snow depth and the corresponding vegetation height. The snow covers of Fool Creek, Saint Louis Creek and Spring Creek exhibit scale breaks at similar scales as the corresponding vegetation fields, while at Buffalo Pass and Walton Creek the scale breaks of the snow depth occur at larger scales with respect to those of the corresponding vegetation height (see Tables 2–4 for snow depth and Tables 5 and 6 for vegetation height). However, there are also important differences in the nature of the variability of snow depth between these two groups. Examination of the snow depth rasters of the study areas (not shown) indicates that the snow covers of Fool Creek, Saint Louis Creek and Spring Creek are exposed to little or no wind redistribution, and small-scale variability consistent with the vegetation patterns is dominant. On the other hand, the snow covers of the Buffalo Pass and Walton Creek exhibit patterns of drifts and scour areas consistent with the location of obstacles such as vegetation and ridges with respect to the predominant wind directions. To illustrate the importance of wind-driven snow redistribution in the study areas, wind data at 1 m above maximum expected snow depth (lower sensor) and 10 m above the ground (upper sensor) for the period October 2002 to April 2003 were analyzed. This period is chosen to represent the meteorological characteristics between the first snowfalls and the time at which the LIDAR snow depths were obtained. These meteorological data were collected as part of the CLPX within each of the ISA's at towers located approximately in the center of each area. Given that snow redistribution due to wind is only likely to occur when the air temperature is below freezing, only maximum wind speeds for 10-min intervals with air temperature less than 0°C are analyzed. The empirical distribution functions of the maximum wind speeds at the lower and upper sensors are shown in Figure 6. The average maximum wind speeds at the lower and upper sensors are 0.8 m/s and 1.8 m/s at Fool Creek, 0.4 m/s (both levels) at Saint Louis Creek, 2.3 m/s and 2.6 m/s at Spring Creek, while they are 3.5 m/s and 4.4 m/s at Buffalo Pass, and 3.8 m/s and 4.4 m/s at Walton Creek, respectively. The empirical distributions indicate higher wind speed regimes at the last two areas, consistent with the observed patterns of snowdrifts and scour areas in the snow depth rasters.

[30] With respect to the vegetation topography (topography + vegetation height) data, the variogram analysis of *Deems et al.* [2006] indicates the existence of a scale break at distances

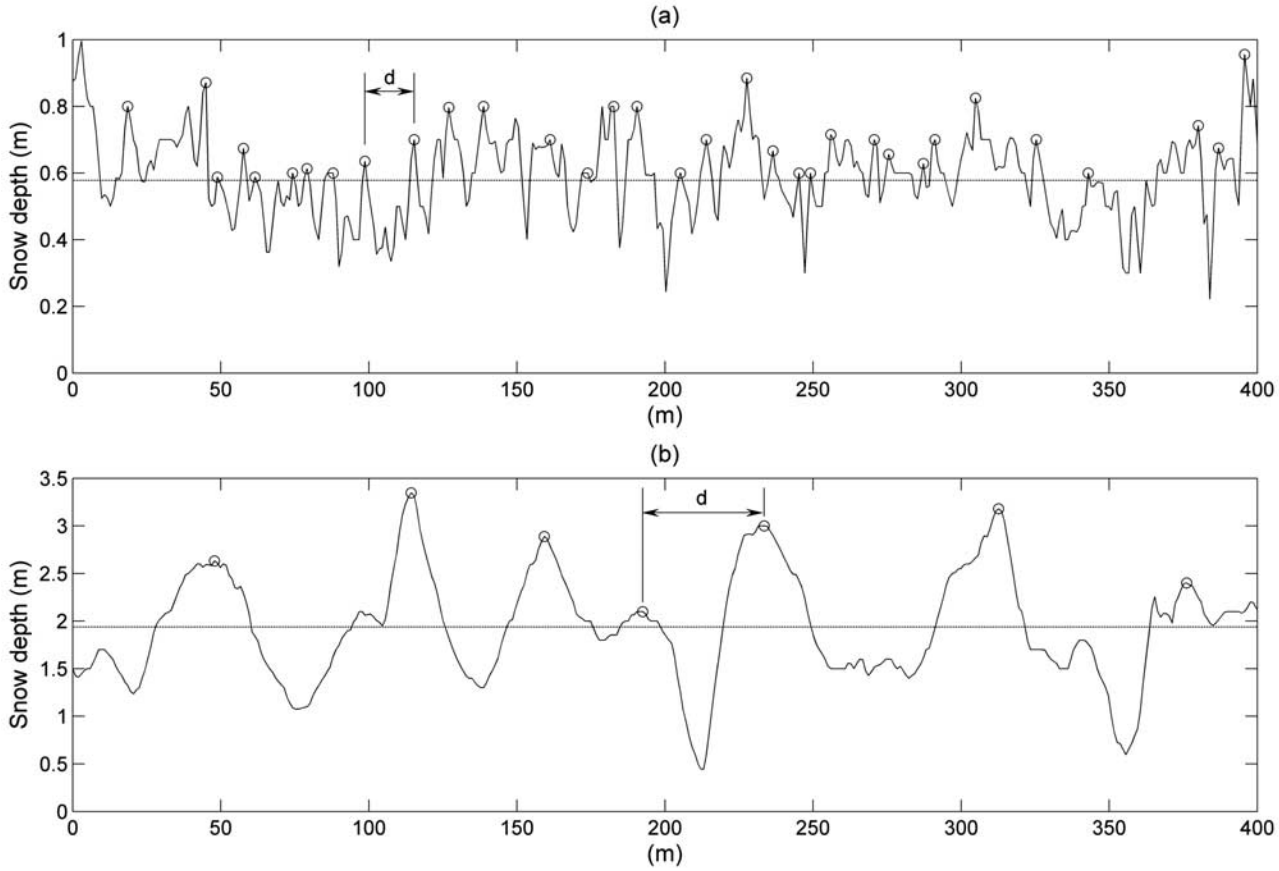

Figure 7. Sample profiles of snow depth at (a) St. Louis Creek and (b) Walton Creek. The circled points mark the location of the local maxima using a threshold equal to the average of the profile. The separation "d" marks the distance between these peaks.

of the same order of magnitude as those observed in the snow depth variograms, though at a slightly longer absolute range. On the other hand, their variograms of vegetation height data (vegetation topography with bare earth terrain subtracted) do not display a scale break. Deems et al. conclude that the similarity between the scale break separating the two regions in the terrain–vegetation distributions and that observed in the snow depth data indicates that the process change revealed in the vegetation–terrain data potentially influences the scaling behavior of snow depth patterns. These observations are contrary to what is observed in the power spectral analysis presented in this study. As mentioned above, no scale breaks are observed in the spectra of topography + vegetation. On the other hand, the spectral densities of vegetation height for all of the study sites exhibit a break at wavelengths between 7 m and 16 m. The locations of the scale breaks in the power spectra of vegetation height coincide with the breaks in the spectra of snow depth only in the areas in which little redistribution of snow by wind exists, and small-scale variability consistent with the vegetation patterns is dominant. On the other hand, the scale breaks in the snow depth spectra in the areas where snow redistribution by wind is dominant are located at larger spatial scales than those of the corresponding vegetation.

[31] In order to compare the characteristics of the variability of the snow depth cover between these two environments, two sample profiles of snow depth of the Saint Louis Creek and Walton Creek snow covers are presented in Figure 7. The differences in the variability of the profiles are evident. The Saint Louis Creek snow cover is characterized by small-scale variations and lower variance (compare the vertical scales), while the snow cover at Walton Creek exhibits larger-scale variations and higher variance. In Figure 7, "d" is defined as the separation distance between peaks (or local maxima) above a threshold equal to the mean snow depth of the profile. The Walton Creek profile exhibits larger separations as a sign of larger characteristic scales. On the basis of this definition, the empirical distribution functions of the separation distance "d" were obtained using all of the profiles in each of the snow depth fields in the x and y directions (Figure 8). The distributions for the first group have very similar shapes with a marked mode located between 7 m and 10 m, while for the second group they are more uniform, with flatter peaks, and with modes located between 11 m and 16 m. The snow depth surfaces of Buffalo Pass and Walton Creek exhibit larger separations between peaks. These results are consistent with the spectral characteristics of the snow depth fields, for which the breaks in the slope of the log-log spectra occur at larger spatial scales at Buffalo Pass and Walton Creek.

[32] The similarities between the power spectrum of snow depths and vegetation heights at Fool Creek, Saint Louis Creek and Spring Creek indicate similarities in the variability

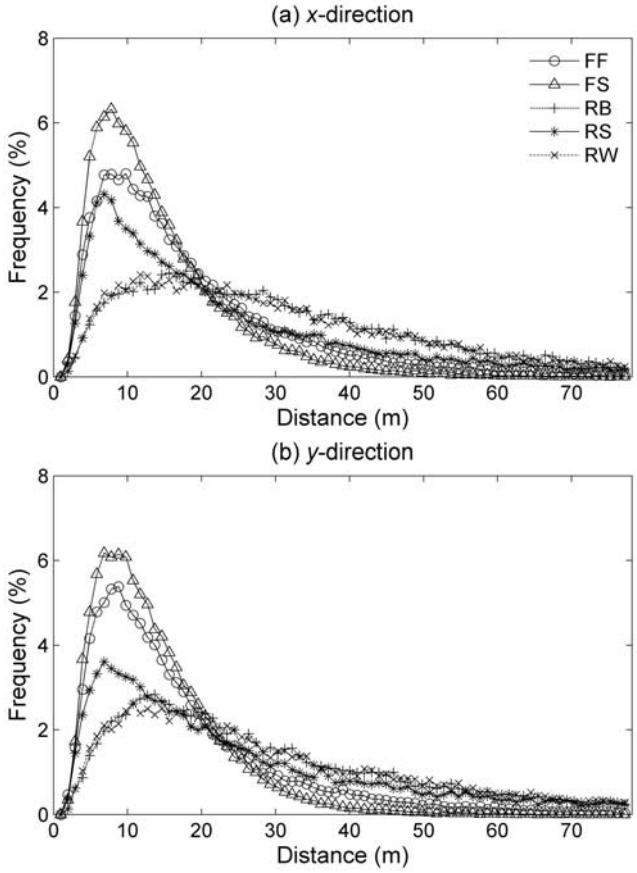

Figure 8. Empirical distribution functions of the separation distance between peaks in the snow depth profiles.

of the two corresponding fields. The empirical distribution functions of the separation distance in the vegetation height and snow depth fields of these study areas (Figure 9) have very similar characteristics, with gamma-type distributions and modes located within similar separation ranges (from 5 m to 8 m for vegetation height and from 7 m to 10 m for snow depth). The separations between peaks in both of the fields exhibit similar statistical characteristics, indicating similar characteristic scales. These similarities are a consequence of the effect of vegetation in the distribution of snow depth. Because of interception, the peaks (maxima) in vegetation height coincide with valleys (minima) in the snow depth surface, and the information that their corresponding separation distances provide about the scales of the variations is statistically equivalent in both fields. As wind redistribution is minimal in these areas, the characteristic scales of snow depths remain similar to those of the vegetation heights.

[33] The directional analysis of the snow depth spectra (Figure 3) indicates higher directionality in the Buffalo Pass and Walton Creek snow depths, with the largest variations in the low-frequency exponents and scale breaks with direction. These variables are compared to the distributions of wind direction for the period October 2002 to April 2003 in Figure 10. The distributions represent the percentage of time that wind blows along a specific line (either direction). Both the low-frequency exponent and scale break exhibit a strong relationship with the predominant wind directions. The lowest low-frequency exponents occur along the predominant wind directions while the highest occur along the perpendicular to the predominant direction. This relationship implies that the snow depth profiles are more variable (rougher) along the predominant wind directions when looked at scales larger than the corresponding scale break. Lower spectral exponents imply a more horizontal slope in the log-log spectrum and higher contributions of the low frequencies to the variance of the profiles. Along the predominant wind direction, most of the variations in snow depth caused by redistribution are a consequence of the vertical interaction of wind patterns with obstacles such as ridges, depressions, and clusters of vegetation. Along the perpendicular direction, a switch in the processes occurs and most of the variations in snow depth caused by redistribution are a consequence of horizontal interactions of wind patterns with obstacles such as trees and rocks. The characteristic scales of such processes depend mainly on the separation distance between obstacles, wind velocities (speed and direction) and surface conditions (e.g., cohesion and roughness). The differences between these processes translate in anisotropy and directionality of the snow depth surface. The results obtained in this study are a consequence and evidence of such directional effect, and the gradual variation of the scaling properties of snow depth in wind-dominated environments (Figure 10) is a consequence of the combination of the vertical and horizontal interaction of wind patterns with obstacles along directions between the predominant and perpendicular directions. The results presented in Figure 3 also indicate little or no directionality in the spectral properties of snow covers with little or no redistribution. The spectral exponents and scale breaks for the snow covers of Fool Creek, Saint Louis Creek and Spring Creek exhibit little variations with direction. The characteristics of the variability of snow depth are relatively similar along any direction, as snow redistribution by wind does not cause extended patterns of snowdrifts and scour areas along any particular direction.

[34] For Buffalo Pass and Walton Creek, *Deems et al.* [2006] report that for distances shorter than the scale break, the snow depth fractal dimensions are larger in directions normal to the prevailing winds, while for longer scales, the largest dimensions occur parallel to the dominant wind direction. However, the variations in the fractal dimensions reported by Deems et al. without indicating their significance level are of the order of 0.1 or less for the two scale regions, variations that might be easily induced by small changes in the number of data used for the regressions. In this study, consistent variations with direction at the Buffalo Pass and Walton Creek ISA's were only observed in the spectral exponents of larger-scale intervals and the locations of the scale breaks. Little variations were observed in the spectral exponent of the smaller-scale intervals (Figures 3 and 10).

[35] A hypothesis proposed first by *Shook and Gray* [1996], and adopted later by *Deems et al.* [2006], to explain the bilinear behavior of the spatial scaling of the distribution of snow depth relates the scale break distance to topographic relief. The results presented in this study reveal that relief does not play a significant role in the observed scaling behavior of the spatial distribution of snow depth, and instead, variables such as vegetation and winds are far more

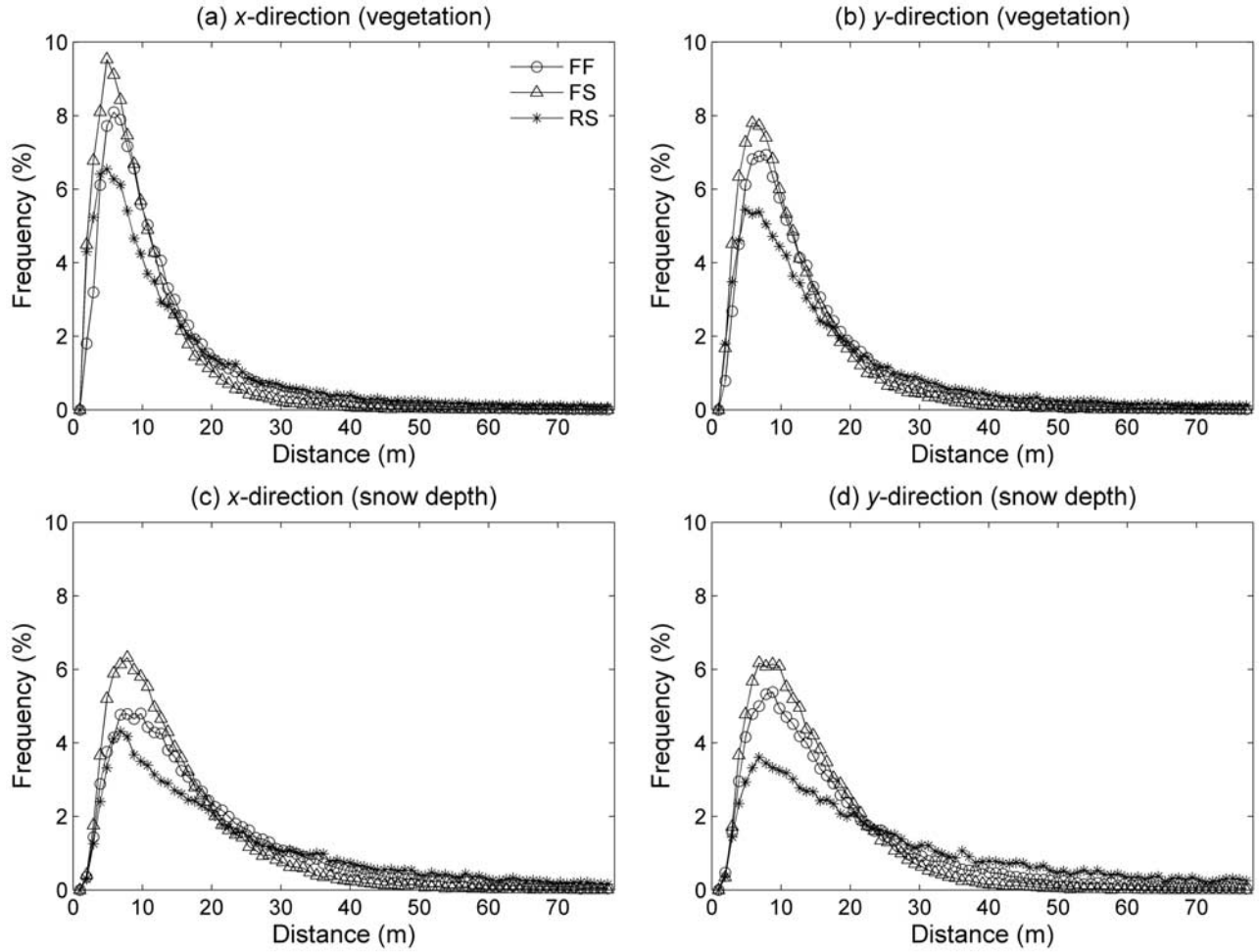

Figure 9. Empirical distribution functions of the separation distance between peaks in the vegetation height and snow depth profiles of the Fool Creek, St. Louis Creek, and Spring Creek ISA's.

relevant when explaining such behavior within the range of scales analyzed.

[36] The differences between the two scaling regimes (i.e., low and high frequencies) in the snow depth fields have important consequences for the characterization of the snow cover. As discussed earlier, the scale break is a measure of the separation between peaks in the snow depth surface. When the snow depth surface is analyzed above such scales, the average effects of the controlling variables need to be accounted for. Such effects correspond to the average snowfall interception by vegetation in environments dominated by canopy interception of snowfall, and the average accumulation or scour induced by redistribution of snow in wind-dominated environments. When the snow cover is looked at scales smaller than the corresponding break, the detailed characteristics (variability between peaks) become evident, and the small-scale interactions become dominant (e.g., vegetation interception by individual trees and wind interaction with surface concavities, trees and rocks). The scales at which snow models work should be selected according to such characteristic scales. Unless the available input data allows for an accurate representation of the small-scale interactions, model scales should be selected within the low-frequency (larger-scale) range. The results presented here indicate that such scales should exceed 10 m in environments where snow redistribution is minimal, and between 20 m and 40 m in environments where wind redistribution is dominant. These scales are expected to change according to the particular characteristics of each environment, so the values presented in this paper should be used only as reference scales.

6. Conclusions

[37] LIDAR snow depths, bare ground elevations and elevations filtered to the top of vegetation obtained in April and September of 2003 were analyzed to characterize the spatial variability of snow depth. On the basis of the characteristics of the power spectral densities of these fields, the relationship of such variability to influencing factors such as topography and vegetation was defined. The power spectra of snow depth behave as $k^{-\beta}$ within two distinct frequency intervals, each with different spectral exponent. The one-dimensional spectral exponents obtained for snow depth vary between 0.1 and 1.4 for the low-frequency intervals, and between 2.9 and 3.6 for the high-frequency intervals, while the exponents of the mean two-dimensional power spectra vary between 1.3 and 2.2 for the low frequencies, and between 4.0 and 4.5 for the high frequencies. Such values indicate that the snow depth surface is

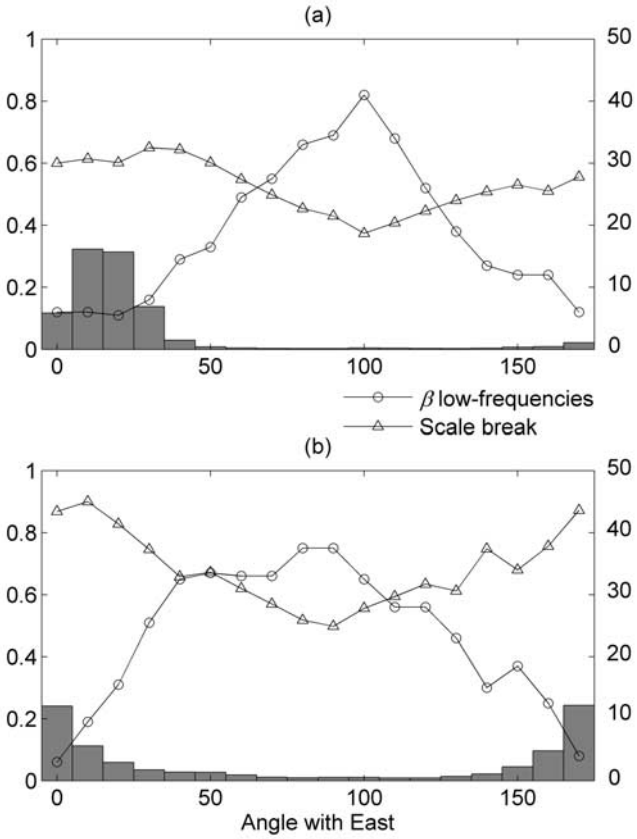

Figure 10. Spectral exponents for the low-frequency intervals (left axis) and scale breaks (right axis (m)) as a function of direction for the (a) Buffalo Pass and (b) Walton Creek ISA's. The histograms correspond to wind directions during intervals with air temperatures below freezing. Similar histograms of wind direction are obtained for wind speeds above thresholds of 4 m/s and 5 m/s.

more variable (or rougher) when observed at scales larger than the corresponding scale break, while much smaller variations appear when looked at scales smaller than such break. The larger scales explain the majority of the variability. The scales that separate these two intervals are located at wavelengths between 8 m and 45 m. None of the scale breaks in the snow depth power spectra were observed in the power spectra of bare ground elevation, or in the spectra of topography + vegetation. Neither the power spectrum exponents nor the scale breaks can be explained on the basis of the power spectrum of the underlying topography and topography + vegetation. On the other hand, the spectrum of vegetation height exhibits very similar behavior as the snow depth spectrum, with a low-frequency interval with mild slopes between 0.3 and 1.2 for the one-dimensional spectra, and between 1.1 and 2.0 for the mean two-dimensional spectra, and a high-frequency interval with steeper slopes between 1.9 and 3.4 for the one-dimensional spectra, and between 2.9 and 4.3 for the mean two-dimensional spectra. These two intervals are separated by a scale break located between 7 m and 16 m for the one-dimensional spectra, and between 7 m and 11 m for the mean two-dimensional spectra.

[38] When the spectra of snow depth are compared to the spectra of the corresponding vegetation height, two distinct scaling behaviors can be identified. In the areas in which snowfall interception is dominant and snow redistribution by wind is minimal, the scale breaks in the snow depth spectra occur at similar scales as those of the corresponding vegetation. On the other hand, in areas where snow redistribution by wind is dominant, the scale breaks in the snow depth spectra are displaced toward scales larger than those of the corresponding vegetation. Redistribution of snow by wind leads to the formation of snowdrifts and scour areas over larger scales, affecting the scaling characteristics of the snow depth surface after the snow is initially deposited. The scales at which the switch in the scaling properties of snow depth occurs are comparable to the separation distance between peaks (local maxima above a threshold) in the snow depth profiles. These characteristics support the conclusion that the break in the scaling behavior of snow depth is controlled by the vegetation characteristics (e.g., height, area covered by the canopy, and separation between trees) when wind redistribution is minimal and canopy interception is dominant, and by the interaction of winds with features such as surface concavities and vegetation when wind redistribution is dominant. Such effect of wind redistribution is also evidenced in the directional spectra, with the lowest low-frequency exponents and the largest scale breaks occurring along the predominant wind directions, as sign of scaling anisotropy and directionality in wind-dominated environments. Until this study, evidence of the links between these processes and the scaling behavior observed in the power spectrum of snow depth in these two types of environments had not been provided.

[39] The results obtained in this study have important implications with respect to processes, measurement and model scales. The existence of a break in the scaling of snow depth at scales of the order of meters to tens of meters indicates a switch in the characteristics of the variability above and below the break. Within each scale interval, similar processes are controlling the variability as indicated by the power law relationship that characterizes the spectrum within each range. If the objective is to reveal small-scale processes such as vegetation interception by individual trees and wind interaction with small features such as surface concavities, trees and rocks, measurement and model scales should be selected within the high-frequency range. In this way, the details of the snow depth surface between the peaks can be revealed. If the objective is to represent the average effect of processes such as canopy interception of snowfall and snow redistribution due to wind, measurement and model scales should be selected within the low-frequency range. For practical purposes in hydrologic applications, accurate description of the small-scale interactions might not be necessary and the detailed information required to reproduce such processes might not be available. Model and measurement scales should be selected according to such objectives. Further analysis of spatially distributed data for different times in the season and larger spatial scales is required to expand the characterization of the variability of snow properties.

Appendix A

[40] Scale invariant systems are systems whose (statistical) properties at different scales are related by a scale-changing

operation involving only a scale ratio. Statistical scale invariance can be expressed as [e.g., *Voss*, 1985b]

$$[V(t+b\Delta t)-V(t)]^d = b^H[V(t+\Delta t)-V(t)] \quad \text{(A1)}$$

where b is a scale factor, H is the Hausdorff exponent, and $\stackrel{d}{=}$ indicates that the two sides of the expression possess the same probability distribution function. Self-similarity corresponds to the particular case of H equal to 1, implying isotropic rescaling for the two coordinates, t and V. On the other hand, self-affinity corresponds to the case in which each coordinate is rescaled by a different scale ratio, i.e., H other than 1. These concepts can be extended to higher Euclidian dimensions by replacing t with a more general vector $\mathbf{x} = (x_1, x_2, \ldots, x_E)$ in an E dimensional space, leading to the following expression [e.g., *Voss*, 1985a, 1985b]:

$$[V(\mathbf{x}+b\Delta\mathbf{x})-V(\mathbf{x})]^d = b^H[V(\mathbf{x}+\Delta\mathbf{x})-V(\mathbf{x})] \quad \text{(A2)}$$

[41] Equation (A2) implies scaling isotropy along the coordinates of the vector $\mathbf{x}$ as the exponent H is constant along any component of $\mathbf{x}$ but allows for scaling anisotropy (i.e., self-affinity) with respect to V as H may be different from 1. Scaling anisotropy or self-affinity may arise when the coordinates are not equivalent (e.g., $\mathbf{V}$ and $\mathbf{x}$, or $\mathbf{x}$ and t), or when different processes affect the variability along different directions. Such anisotropy can be analyzed by looking at the scaling properties (e.g., spectral exponent) along each coordinate independently or by analyzing the changes of such properties along different directions (e.g., different combinations of x and y).

[42] For a self-affine function of one variable (e.g., t as in (A1)) the power spectral density $P(k)$ follows a power law dependence on the wave number k as [e.g., *Voss*, 1985a, 1985b]

$$P(k) \propto k^{-\beta} \quad \text{(A3)}$$

[43] Similarly, the two-dimensional power spectra of self-affine functions in the x-y plane where all directions in the x-y plane are equivalent also obey a power law as

$$P(k) \propto \left(k_x^2 + k_y^2\right)^{-\beta/2} = (k)^{-\beta}$$
$$k = \left(k_x^2 + k_y^2\right)^{1/2} \quad \text{(A4)}$$

but with a spectral exponent that differs by 1 with respect to the corresponding one-dimensional exponent [e.g., *Voss*, 1985b]. Also observe that now k stands for a general wave number. A more general form of (A4) allows also for scaling anisotropy along each of the components of the vector $\mathbf{x}$ as [e.g., *De Michele and Bernardara*, 2005]

$$P(k_x, k_y) \propto \left(\alpha_x^2 k_x^2 + \alpha_y^2 k_y^2\right)^{-\beta/2} \quad \text{(A5)}$$

[44] In the case of fractional Brownian motion, the one-dimensional spectral exponent and the Hausdorff exponent are related as [e.g., *Voss*, 1985a, 1985b]

$$\beta = 2H + 1 \quad \text{(A6)}$$

[45] The spectral exponent can be used as a measure of the persistence for all values of β. Functions with low spectral exponents are highly variable and adjacent values are less correlated. As the exponent increases, the functions become smoother and adjacent values become more correlated. Low spectral exponents imply a more uniform contribution of all frequencies to the variability of the series, leading to a "rougher" pattern with high-frequency (short wavelengths) variations of similar orders of magnitude as the low-frequency variations (long wavelengths). As the exponent increases, the contributions of the low frequencies become increasingly dominant over the contributions of the short frequencies, and as a consequence the correlation between adjacent values of the series increases and the profile becomes smoother. Weak long-range persistence corresponds to $0 < \beta < 1$, whereas strong long-range persistence corresponds to $\beta > 1$. The value of the spectral exponent also has important implications with respect to the convergence or divergence of the variance [e.g., *Malamud and Turcotte*, 1999]. The variance converges for $\beta < 1$, and diverges for $\beta > 1$. Self-affine time series with $\beta < 1$ are stationary while series with $\beta > 1$ are nonstationary, and $\beta = 1$ can be used as a crossover between weak and strong persistence in time series [*Malamud and Turcotte*, 1999].

[46] Spectral techniques are often preferred over other techniques, such as variogram analysis, for the study of the scaling properties of random fields. This is because, depending on the value of β, different techniques are more or less accurate in estimating the scaling properties of fields. In the case of variogram analysis, the range of β for which one can expect reasonably accurate results is $1.2 < \beta < 2.5$, whereas spectral techniques are accurate for all values of β [e.g., *McSharry and Malamud*, 2005]. Spectral techniques have been used to explore the scaling characteristics of highly variable processes such as rainfall rate [e.g., *Crane*, 1990; *Veneziano et al.*, 1996], topography [e.g., *Brown*, 1987; *Turcotte*, 1987, 1989; *Huang and Turcotte*, 1989], soil moisture [*Kim and Barros*, 2002], and groundwater base flow [e.g., *Zhang and Schilling*, 2004; *Zhang and Li*, 2005].

[47] **Acknowledgments.** Support for this research was provided by the USDA-USFS Rocky Mountain Research Station under contract 04-JV-11221610-029. Base funding was provided by NASA under contract 02-IA-11221610-104.

References

Arnold, N. S., and W. G. Rees (2003), Self-similarity in glacier surface characteristics, *J. Glaciol.*, *49*(167), 547–554.

Blöschl, G. (1999), Scaling issues in snow hydrology, *Hydrol. Processes*, *13*(14–15), 2149–2175.

Blöschl, G., and R. Kirnbauer (1992), An analysis of snow cover patterns in a small alpine catchment, *Hydrol. Processes*, *6*(1), 99–109.

Brown, S. R. (1987), A note on the description of surface roughness using fractal dimension, *Geophys. Res. Lett.*, *14*(11), 1095–1098.

Crane, R. (1990), Space-time structure of rain rate fields, *J. Geophys. Res.*, *95*, 2011–2020.

Deems, J. S., S. R. Fassnacht, and K. J. Elder (2006), Fractal distribution of snow depth from LIDAR data, *J. Hydrometeor.*, *7*(2), 285–297.

De Michele, C., and P. Bernardara (2005), Spectral analysis and modeling of space-time rainfall fields, *Atmos. Res.*, *77*, 124–136.

Elder, K., J. Dozier, and J. Michaelsen (1991), Snow accumulation and distribution in an alpine watershed, *Water Resour. Res.*, *27*, 1541–1552.

Elder, K., J. Michaelsen, and J. Dozier (1995), Small basin modeling of snow water equivalence using binary regression tree methods, in *Proceedings of the Symposium on Biogeochemistry of Seasonally Snow Covered Catchments*, *IAHS-AIHS and IUGG XX General Assembly*, *IAHS Publ.*, *228*, 129–139.

Elder, K., W. Rosenthal, and R. Davis (1998), Estimating the spatial distribution of snow water equivalence in a montane watershed, *Hydrol. Processes*, *12*(10–11), 1793–1808.

Erickson, T. A., M. W. Williams, and A. Winstral (2005), Persistence of topographic controls on the spatial distribution of snow in rugged mountain terrain, Colorado, United States, *Water Resour. Res.*, *41*, W04014, doi:10.1029/2003WR002973.

Erxleben, J., K. Elder, and R. Davis (2002), Comparison of spatial interpolation methods for estimating snow distribution in the Colorado Rocky Mountains, *Hydrol. Processes*, *16*(18), 3627–3649.

Evans, B. M., D. A. Walker, D. S. Benson, E. A. Nordstrand, and G. W. Petersen (1989), Spatial interrelationships between terrain, snow distribution and vegetation patterns at an artic foothills site in Alaska, *Holarctic Ecol.*, *12*, 270–278.

Granger, R. J., J. W. Pomeroy, and J. Parviainen (2002), Boundary-layer integration approach to advection of sensible heat to a patchy snow cover, *Hydrol. Processes*, *16*(18), 3559–3569.

Greene, E. M., G. E. Liston, and R. A. Pielke Sr. (1999), Relationships between landscape, snow cover depletion, and regional weather and climate, *Hydrol. Processes*, *13*(14), 2453–2466.

Hosang, J., and K. Dettwiler (1991), Evaluation of a water equivalent of snow cover map in a small catchment-area using geostatistical approach, *Hydrol. Processes*, *5*(3), 283–290.

Huang, J., and D. L. Turcotte (1989), Fractal mapping of digitized images: Application to the topography of Arizona and comparison with synthetic images, *J. Geophys. Res.*, *94*, 7491–7495.

Kang, B. and J. A. Ramírez (2001), Comparative study of the statistical features of random cascade models for spatial rainfall downscaling, in *Proceedings of AGU Hydrology Days 2001*, edited by J. A. Ramírez, pp. 151–164, Hydrol. Days, Fort Collins, Colo.

Kim, G., and A. P. Barros (2002), Downscaling of remotely sensed soil moisture with a modified fractal interpolation method using contraction mapping and ancillary data, *Remote Sens. Environ.*, *83*(2), 400–413.

Kuchment, L. S., and A. N. Gelfan (2001), Statistical self-similarity of spatial variations of snow cover: Verification of the hypothesis and application in the snowmelt runoff generation models, *Hydrol. Processes*, *15*(18), 3343–3355.

Liston, G. E. (1999), Interrelationships among snow distribution, snowmelt, and snow cover depletion: Implications for atmospheric, hydrologic, and ecologic modeling, *J. Appl. Meteorol.*, *38*(10), 1474–1487.

Liston, G. E., and M. Sturm (1998), A snow-transport model for complex terrain, *J. Glaciol.*, *44*(148), 498–516.

Liston, G. E., R. A. Pielke Sr., and E. M. Greene (1999), Improving first-order snow-related deficiencies in a regional climate model, *J. Geophys. Res.*, *104*, 19,559–19,567.

Lovejoy, S., and D. Schertzer (1985), Generalized scale invariance in the atmosphere and fractal models of rain, *Water Resour. Res.*, *21*, 1233–1240.

Luce, C. H., and D. G. Tarboton (2001), Modeling snowmelt over an area: Modeling subgrid scale heterogeneity in distributed model elements, paper presented at MODSIM 2001, International Congress on Modeling and Simulation, Modell. and Simul. Soc. of Aust. and N. Z. Inc., Canberra, Australia, 10–13 Dec.

Luce, C. H., and D. G. Tarboton (2004), The application of depletion curves for parameterization of subgrid variability of snow, *Hydrol. Processes*, *18*(8), 1409–1422.

Luce, C. H., D. G. Tarboton, and K. R. Cooley (1997), Spatially distributed snowmelt inputs to a semi-arid mountain watershed, paper presented at *Western Snow Conference*, Banff, Canada, 5–8 May.

Luce, C. H., D. G. Tarboton, and K. R. Cooley (1998), The influence of the spatial distribution of snow on basin-averaged snowmelt, *Hydrol. Processes*, *12*(10), 1671–1683.

Luce, C. H., D. G. Tarboton, and K. R. Cooley (1999), Sub-grid parameterization of snow distribution for an energy and mass balance snow cover model, *Hydrol. Processes*, *13*(12–13), 1921–1933.

Malamud, B. D., and D. L. Turcotte (1999), Self-affine time series: Measures of weak and strong persistance, *J. Stat. Plann. Inference*, *80*, 173–196.

Mandelbrot, B. (1967), How long is the coast of Britain? Statistical self-similarity and fractional dimension, *Science*, *156*(3775), 636–638.

Mandelbrot, B. (1982), *The Fractal Geometry of Nature*, 468 pp., W. H. Freeman, San Francisco, Calif.

Marsan, D., D. Schertzer, and S. Lovejoy (1996), Causal space-time multifractal processes: Predictability and forecasting of rain fields, *J. Geophys. Res.*, *101*, 26,333–26,346.

McSharry, P. E., and B. D. Malamud (2005), Quantifying self-similarity in cardiac inter-beat interval time series, *Comput. Cardiol.*, *32*, 459–462.

Meng, H., J. A. Ramírez, J. D. Salas, and L. Ahuja (1996), Scaling analysis of infiltration at R-5 catchment, in *Invited Proceedings of the USDA-ARS Workshop on Real World Infiltration*, *CWRRI Inf. Ser. 86*, pp. 239–240, Colo. Water Resour. Res. Inst., Fort Collins.

Miller, S. L. (2003), CLPX-Airborne: Infrared Orthophotography and LIDAR Topographic Mapping, Natl. Snow and Ice Data Center, Digital Media, Boulder, Colo.

Molnar, P., and J. A. Ramírez (1998), Energy dissipation theories and optimal channel characteristics of river networks, *Water Resour. Res.*, *34*, 1809–1818.

Over, T. M. (1995), Modeling space-time rainfall at the mesoscale using random cascades, Ph.D. thesis, Univ. of Colo., Boulder.

Over, T. M., and V. K. Gupta (1996), A space-time theory of mesoscale rainfall using random cascades, *J. Geophys. Res.*, *101*, 26,319–26,332.

Rodríguez-Iturbe, I., and A. Rinaldo (1996), *Fractal River Basins*, 564 pp., Cambridge Univ. Press, Cambridge, U.K.

Rodríguez-Iturbe, I., G. K. Vogel, R. Rigon, D. Entekhabi, F. Castelli, and A. Rinaldo (1995), On the spatial organization of soil moisture fields, *Geophys. Res. Lett.*, *22*(20), 2757–2760.

Shook, K., and D. M. Gray (1994), Determining the snow water equivalent of shallow prairie snow covers, paper presented at 51st Eastern Snow Conference, Dearborn, Mich., 14–16 Jun.

Shook, K., and D. M. Gray (1996), Small-scale spatial structure of shallow snow covers, *Hydrol. Processes*, *10*(10), 1283–1292.

Shook, K., and D. M. Gray (1997), Synthesizing shallow seasonal snow covers, *Water Resour. Res.*, *33*, 419–426.

Shook, K., D. M. Gray, and J. W. Pomeroy (1993), Temporal variation in snow cover area during melt in Prairie and Alpine environments, *Nord. Hydrol.*, *24*, 183–198.

Tarboton, D. G., R. L. Bras, and I. Rodríguez-Iturbe (1988), The fractal nature of river networks, *Water Resour. Res.*, *24*, 1317–1322.

Tessier, Y., S. Lovejoy, and D. Schertzer (1993), Universal multifractals: Theory and observations for rain and clouds, *J. Appl. Meteorol.*, *32*(2), 223–250.

Turcotte, D. L. (1987), A fractal interpretation of topography and geoid spectra on the Earth, Moon, Venus, and Mars, *Proc. Lunar Planet. Sci. Conf. 17th*, Part 2, *J. Geophys. Res.*, *92*, suppl., E597–E601.

Turcotte, D. L. (1989), Fractals in geology and geophysics, *Pure Appl. Geophys.*, *131*(1), 171–196.

Veneziano, D., and V. Iacobellis (1999), Self-similarity and multifractality of topographic surfaces at basin and subbasin scales, *J. Geophys. Res.*, *104*, 12,797–12,812.

Veneziano, D., R. L. Bras, and J. D. Niemann (1996), Nonlinearity and self-similarity of rainfall in time and a stochastic model, *J. Geophys. Res.*, *101*, 26,371–26,392.

Voss, R. F. (1985a), Random fractals: Characterization and measurement, in *Scaling Phenomena in Disordered Systems*, edited by R. Pynn and A. Skjeltorp, pp. 1–11, Plenum, New York.

Voss, R. F. (1985b), Random fractal forgeries, in *Fundamental Algorithms for Computer Graphics*, *NATO ASI Ser.*, vol. F17, edited by R. A. Earnshaw, pp. 805–835, Springer, Berlin, Germany.

Winstral, A., K. Elder, and R. Davis (2002), Spatial snow modeling of wind-redistributed snow using terrain-based parameters, *J. Hydrometeorol.*, *3*(5), 524–538.

Zhang, Y. K., and Z. Li (2005), Temporal scaling of hydraulic head fluctuations: Nonstationary spectral analyses and numerical simulations, *Water Resour. Res.*, *41*, W07031, doi:10.1029/2004WR003797.

Zhang, Y. K., and K. Schilling (2004), Temporal scaling of hydraulic head and river base flow and its implication for groundwater recharge, *Water Resour. Res.*, *40*, W03504, doi:10.1029/2003WR002094.

K. J. Elder, Rocky Mountain Research Station, USDA Forest Service, 240 West Prospect Road, Fort Collins, CO 80526 USA.

J. A. Ramírez and E. Trujillo, Department of Civil and Environmental Engineering, Colorado State University, Fort Collins, CO 80523-1372, USA. (etrujil@engr.colostate.edu)